

<https://doi.org/10.1038/s42003-025-07765-x>

Mapk7 enhances osteogenesis and suppresses adipogenesis by activating Lrp6/ β -catenin signaling axis in mesenchymal stem cells




Chuan Li^{1,2,6}, Jiahui Long^{1,6}, Shuqing Chen^{3,6}, Liru Tian^{1,4}, Ya Xiao¹, Shulin Chen¹, Deying Su¹, Baolin Zhang⁵, Peiqiang Su⁵ , Liao Zhiheng ⁵  & Caixia Xu ¹ 

The lineage commitment and differentiation of mesenchymal stem cells (MSCs) play a crucial role in bone homeostasis. MAPK7 (Mitogen-activated protein kinase 7), a member of MAPK family, controls cell differentiation, proliferation and survival. However, the specific role of Mapk7 in regulating osteogenic and adipogenic differentiation of MSCs remains to be determined. In this study, depletion of *Mapk7* in MSCs by crossing *Prx1*-Cre mice to *Mapk7*^{flox/flox} resulted in severe low bone mass and accumulation of fat in bone marrow exhibiting osteoporosis (OP) in mice. Mapk7 promoted osteogenic differentiation and inhibited adipogenic differentiation of MSCs after knocking out and over-expressing *Mapk7* in vitro. Mechanistically, Mapk7 activated Wnt/ β -catenin signaling by phosphorylating Lrp6 at Ser1490, which ultimately enhanced osteogenesis and suppressed adipogenesis of MSCs. This is of great clinical and scientific significance for understanding biological function of Mapk7 and developing potential therapeutic targets for treatment of MSCs differentiation imbalance related bone diseases, such as, osteoporosis.

Mesenchymal stem cells (MSCs) are a class of mesodermal derived stem cells that served as a pool of multipotent progenitors, which have the potential to differentiate exclusively into either osteogenesis or adipogenesis lineages, isolated from a variety of adult or fetal tissues^{1–6}. As a common progenitor of adipocytes and osteoblasts, the tightly controlled lineage commitment of MSCs play a critical role in the maintenance of bone homeostasis⁷. With age and estrogen deficiency, MSCs preferentially differentiate into adipocytes, resulting in increasing in bone marrow fat and progressive bone loss, which lead to a series of complications such as increased bone fragility and fracture^{8,9}. Therefore, searching for key factors that promote osteogenic differentiation of MSCs while inhibiting adipogenic differentiation is a potential endeavor for OP.

Recent findings suggested that many transcription factors, signaling pathways, epigenetic regulation, and other factors played key roles in

regulating the lineage commitment of MSCs, and alteration of these factors contributed to the imbalance of osteogenic and adipogenic differentiation of MSCs resulting OP^{10,11}. Decades of in-depth studies have demonstrated that mitogen-activated protein kinases (MAPKs), Wntless-Type MMTV Integration Site Family (Wnt)/ β -catenin signaling, bone morphogenetic protein (BMP) pathway, and Notch signaling exhibit dual regulatory functions in modulating MSCs differentiation^{10,11}. This modulation occurs through targeting downstream transcription factors like runt-related transcription factor 2 (Runx2), osterix (Osx), and peroxisome proliferative activated receptor, gamma (Ppar γ), as well as through intricate cross-talk among these signaling pathways^{10,11}. Nonetheless, the mechanisms that govern the imbalance between osteogenic and adipogenic differentiation of MSCs are exceptionally intricate, and numerous pivotal regulators remain undefined, necessitating additional exploration and comprehensive research.

¹Research Center for Translational Medicine, The First Affiliated Hospital of Sun Yat-sen University, 510080 Guangzhou, China. ²Department of Urology, The Second Affiliated Hospital of Guangzhou Medical University, 510260 Guangzhou, China. ³Department of Traditional Chinese Medicine, The First Affiliated Hospital, Sun Yat-sen University, Zhongshan 2 Rd., No. 58, Yuexiu District, 510080 Guangzhou, China. ⁴Department of Pathology, Sun Yat-sen University Cancer Center, 510062 Guangzhou, China. ⁵Guangdong Provincial Key Laboratory of Orthopedics and Traumatology, Department of Spine Surgery, The First Affiliated Hospital of Sun Yat-sen University, 510080 Guangzhou, China. ⁶These authors contributed equally: Chuan Li, Jiahui Long, Shuqing Chen.  e-mail: supq@mail.sysu.edu.cn; liaozh27@mail.sysu.edu.cn; xucx3@mail.sysu.edu.cn

MAPK (ERK) family, containing ERK1 (also known as MAPK3), ERK2 (MAPK1), c-Jun N-terminal kinase (MAPK8/9), and p38 (MAPK14), are crucial in skeletal development and bone mass maintenance, mediating the effects of various extracellular ligands, such as BMPs, WNTs, and parathyroid hormone (PTH), which impact osteogenic potential of MSCs^{12–14}. As one of the less studied and structurally unique members of the MAPK family, MAPK7, also known as ERK5, contains a distinctive C-terminal extension, which encodes two proline-rich domains and incorporates a signal for nuclear localization¹⁵. Mouse genetic studies have revealed its crucial role in heart function via its deletion in the heart, resulting in embryonic lethality¹⁵. Thus, utilizing specific tool mice to investigate its function in particular tissues was a viable solution. Previous research revealed that *MAPK7* was a novel causative gene for adolescent scoliosis (AIS), playing a crucial role in the development of cartilage within the skeletal system; Deletion *MAPK7* impaired osteogenic differentiation potential of human bone marrow-derived MSCs (hBMSCs)¹⁶. Besides, deletion *Mapk7* in chondrocytes (*Col2a1-Cre; Mapk7^{lox/lox}*) impaired endochondral bone formation within the limbs along with bone mass loss¹⁷. Chondrocytes were terminally differentiated cells¹⁷. Therefore, we hypothesize that *Mapk7* may play a role in differentiation in earlier differentiated cells, such as MSCs, and influence skeletal phenotype. Moreover, imbalance between osteogenic and adipogenic differentiation of MSCs was one of the pathological mechanisms of OP^{11,17–19}. However, there is currently a lack of direct evidence regarding the impact of *Mapk7* deficiency, in MSCs fate commitment, as well as its effect on OP. Therefore, elucidating the role of *Mapk7* in MSCs fate transition and its downstream molecular mechanism contributes to refining our understanding of the functions of MAPK family members in maintaining bone homeostasis, as well as provides new insights for related bone disease therapies in the future.

To address the questions above, we crossed *Prx1-Cre* mice with *Mapk7^{lox/lox}* mice to delete *Mapk7* in MSCs and conducted further mechanistic studies using primary MSCs and C3H10T1/2 MSCs. Our results demonstrated that *Prx1-Cre; Mapk7^{lox/lox}* mice exhibited bone loss and increased bone marrow adiposity. Further investigation showed deletion *Mapk7* decreased phosphorylation of Lrp6 at Ser1490 and inhibited Wnt/ β -catenin signaling, thereby suppressing osteogenic differentiation and enhancing adipogenic differentiation of MSCs.

Methods

Animals

Mapk7^{lox/lox} mouse strains were previously described in our study²⁰. *Prx1-Cre* mouse strain were gifted from Bai lab²¹. To generate *Prx1-Cre; Mapk7^{lox/lox}* (conditional knock out, CKO) and *Mapk7^{lox/lox}* (wild type, WT) mice, we used *Mapk7^{lox/lox}* strain mice to cross with *Prx1-Cre* mice. All mice were maintained in an environment with carefully regulated conditions, including temperature (20–26 °C), humidity (40–70%), and lighting. The animal experiments were conducted at the Laboratory Animal Center of Sun Yat-sen University, approved and regulated by the Committee for the Management and Use of Laboratory Animals of Sun Yat-sen University (Approval No. SYSU-IACUC-2022-001823), and all experimental procedures were carried out in compliance with relevant regulations. All efforts were made to minimize animal usage, manipulation, and pain. Mice genotyping was performed by PCR using DNA Extraction Kit and PCR reaction kit (B40015, Selleck, China). The primers used were listed in Supplementary Table 1.

Cell lines and reagents

L Wnt-3A cells (CL-0375, Procell, China) were genetically modified mouse subcutaneous connective tissue cells to stably secrete Wnt3a protein to active Wnt/ β -catenin signaling. L Wnt-3A were cultured in DMEM medium (C11995599BT, Gibco, USA) containing 10% fetal bovine serum (FBS) (A5669701, Gibco, USA). L Wnt-3A was used to co-culture with MSCs in a trans-well plate (TCS016024, JET, China). C3H10T1/2 MSCs were gifted from Wang lab²². CHIR99021 (10 nM; HY-10182A, MCE) was an activator of Wnt/ β -catenin signaling. We added CHIR99021 in the induction

differentiation medium during the differentiation of MSCs to assess the role of Wnt/ β -catenin signaling in *Mapk7* regulation in osteogenesis and adipogenesis of MSCs.

Primary MSCs isolation

Primary mouse MSCs were isolated via flushing bone marrow out of the long bones, digesting the bone chips with collagenase type II, deprivation of the released cells, and culturing the digested bone fragments, out of which fibroblast-like cells migrate and grow in the defined medium as previous described²³. In detail, we isolated primary MSCs by aspirating long bones with a syringe and subsequently digesting bone fragments with type II collagenase (Sigma, V900892-100MG, USA) in a shaker at 37 °C for 2 h. Subsequently, the supernatant was discarded through a centrifuge, and the cellular precipitate, along with bone fragments were collected and re-suspended in α -MEM medium supplemented with 10% FBS. The suspension was cultured for a period of 1–3 days until a sufficient number of large and clonal cell clusters which could be visually confirmed under a microscope. Once the cells reached 80–90% confluence, they were subjected to 0.25% trypsin–EDTA (25200-056, Gibco, USA) digestion, with each digestion step controlled to within 2 min at room temperature. Cells within the passage range of 3–8 were utilized for the procedure.

Flow cytometry

To identify the characteristics of primary MSCs, we detected cell surface markers, such as: CD105-phycoerythrin (PE) (12047, Biolegend, USA), CD29-PE (102207, Biolegend, USA), Sca1-fluorescein isothiocyanate (FITC) (108105, Biolegend, USA), CD45-FITC (103107, Biolegend, USA), CD34-PE (119107, Biolegend, USA) using flow cytometers (CytoFLEX, Beckman Coulter, USA) and analyzing data via FlowJo10.8.1 software.

MSCs differentiation and staining

The differentiation potential of MSCs was further verified by evaluating the multilineage differentiation capabilities in passages 3–6. In details, primary MSCs were cultured in osteogenic/adipogenic induction medium (AIM/OIM) (MUXMX-90031/MUXMX-90031, Cyagen, China). Alkaline phosphatase (ALP) staining was conducted for up to the seventh day of incubation in OIM, as previously described²⁴. Additionally, ARS/ORO staining was performed until visible calcium nodules or oil droplets were observed under a microscope. Calcium nodules were dissolved in DMSO and measured at 405 nm for quantitative analysis. Lipid droplets were extracted using isopropanol, and measured at 510 nm for quantitative analysis. For differentiation to chondrocytes, 1% (vol/vol) Insulin–Transferrin–Selenium (ITS) (41400045, Gibco, USA) was added in α -MEM medium (C12571500BT, Gibco, USA) with 10% (vol/vol) FBS to culture MSCs for 21 days. After the end of chondrogenic differentiation, chondrocytes were stained using alcian blue (ALCB-10001, Cyagen, China) after fixed with 4% PFA (G1101, Servicebio, China).

Real-time quantitative PCR (RT-qPCR) analysis

Total RNA was extracted from cells or tissue using TRIzol reagent (15596-026, Invitrogen, USA) based on manufacturer's protocol. Reverse transcription was conducted using 1–0.5 μ g of RNA and cDNA Synthesis Mix (TSK322S, Tsingke, China) as per the manufacturer's instructions. For RT-qPCR, RTiCanATM SYBR qPCR Mix (TSE501, Tsingke, China) was employed following manufacturer's guidelines. *GAPDH* was utilized as an internal control, and the $2^{-\Delta\Delta Ct}$ method was applied to assess relative gene expression. The primer sequences used for RT-qPCR is provided in Table 1.

Bone tissue imaging and immunological detection

Mouse femur was obtained with removal of muscle tissue, fixed in 4% PFA at 4 °C overnight and stored in 70% ethanol, allowing for direct micro-quantitative computed tomography (μ CT) scanning using a resolution of 10 μ m with a voltage of 70 kV and a current of 200 μ A on a μ CT scanner (SkyScan1276, Bruker, Germany). Bone parameters including bone volume per tissue volume (BV/TV), trabecular thickness (Tb.Th), trabecular number

Table 1 | Primer sequences

Gene	Sequence (5'–3')
<i>Mapk7-F</i>	TAAACCCTCTAACCTTCTGGTCA
<i>Mapk7-R</i>	GAGGTCGATTGCCTGCGTA
<i>Runx2-F</i>	CCAACCGAGTCATTTAAGGCT
<i>Runx2-R</i>	GCTCACGTCGCTCATCTTG
<i>Opn-F</i>	AGCAAGAACTCTTCCAAGCAA
<i>Opn-R</i>	GTGAGATTCTGTCAGATTCATCCG
<i>Alpl-F</i>	CCAACTCTTTGTGCCAGAGA
<i>Alpl-R</i>	GGCTACATTGGTGTGAGCTTTT
<i>Cebpa-F</i>	CAAGAACAGCAACGAGTACCG
<i>Cebpa-R</i>	GTCACCTGGTCAACTCCAGCAC
<i>Cyclinb1-F</i>	AGAGGTGGAACCTTGCTGAGCCT
<i>Cyclinb1-R</i>	GCACATCCAGATGTTTCCATCGG
<i>C-Myc-F</i>	CCTGGTGCTCCATGAGGAGAC
<i>C-Myc-R</i>	CAGACTCTGACCTTTTGCCAGG
<i>Pparγ-F</i>	GGAAGACCACTCGCATTCCTT
<i>Pparγ-R</i>	GTAATCAGCAACCATTTGGGTCA
<i>Fabp4-F</i>	AGCACCATAACCTTAGATGGGG
<i>Fabp4-R</i>	CGTGGAAGTGACGCTTTCA
<i>β-actin-F</i>	GTACGACCAGAGGCATACAGG
<i>β-actin-R</i>	GATGACGATATCGCTGCGCTG
<i>GAPDH-F</i>	AGGTCGGTGTGAACGGATTTG
<i>GAPDH-R</i>	GGGGTCGTTGATGGCAACA

(Tb.N), and the trabecular separation (Tb.Sp) were calculated²⁵, quantifying the trabecular region beneath the growth plate as previously described²⁰. For tibia to be sectioned and stained, decalcification in EDTA for several weeks was conducted, followed by hematoxylin–eosin (H&E) and immunohistochemical (IHC) staining as necessary, rabbit anti-OSX (ab209484, Abcam, IHC: 1:50), mouse anti-OPN (ab69498, Abcam, IHC: 1:50), tartrate-resistant acid phosphatase (TRAP) staining was performed to calculate bone resorption parameter: osteoclast number (N.Oc/BS), which was performed in line with TRAP assay kit procedure (387A-1KT, Sigma, USA).

Dynamic histomorphometry was performed using calcein (C0004-5G, TCL, Japan) (10 mg/kg body weight) and alizarin red S (A3882, Sigma, USA) (20 mg/kg body weight) were injected subcutaneously 12 and 2 days before sacrifice in the 9-week-old mice, respectively. Femur were embedded in methyl methacrylate (M813511-500 ml, Macklin, China), and approximately 100-mm-thick horizontal sections of distal metaphyses and midshaft regions were prepared. Calcein and alizarin red labeling was visualized using a fluorescence microscope (DS-U3, Nikon, Japan) with an excitation wavelength of 450–490 nm and a 510–560 nm band-pass filter, respectively, for clarifying bone formation parameters: mineral apposition rate (MAR) and bone formation rate as bone surface reference (BFR/BS)²⁵.

Western blot (WB) and immunoprecipitation (IP)

Primary MSCs, C3H10T1/2 MSCs were harvested and lysed with RIPA buffer containing 1% phosphatase inhibitor cocktail and protease inhibitor cocktail (HY-K0023-1 mL and HY-K0010-1 mL, MCE, USA) on ice for 20 min. Nuclear lysate of primary MSCs was extracted using Nuclear and Cytoplasmic Protein Extraction Kit (P0028, Beyotime, China) according to operating rules. The lysate was centrifuged at 12,000×g for 15 min at 4 °C. The resulting immunoprecipitation (IP) complexes were prepared using corresponding antibodies according to the instructions provided by Dynabeads™ Protein G (10004D, Thermo Fisher, USA). The complexes were washed and heat denatured, followed by separation of the proteins using SDS–PAGE and transfer onto 0.22 μm PVDF membranes (3010040001, Roche, Germany). After blocking for 1 h at room

temperature, antibody–antigen immunohybridization was performed, and gray-scale detection was carried out using the enhanced chemiluminescence (ECL) detection kit (WBKLS0500, Millipore, USA). GAPDH was used as an internal reference protein. The primary antibodies used were as follows: mouse anti-MAPK7 (3372s, Cell Signaling Technology, WB: 1:200), mouse anti-GAPDH (60004-1-Ig, Proteintech, WB: 1:2000), rabbit anti-RUNX2 (12556, Cell Signaling Technology, WB: 1:1000); mouse anti-OPN (ab69498, Abcam, WB: 1:1000), rabbit non-phospho (Active) anti-β-catenin (19807T, Cell Signaling Technology, WB:1:1000), GSK3β (A11731, Abclonal, WB:1:1000), p-GSK3β (AP1088, Abclonal, WB:1:1000), Phospho-LRP6-S1490 (AP1191, Abclonal, WB:1:1000), LRP6 (A6134, Abclonal, WB:1:1000), MEF2C (10056-1-AP, Proteintech, WB: 1:1000), Phospho-MEF2C (ab78888, Abcam, WB: 1:1000).

Immunofluorescence (IF) staining

Cells were fixed with 4% PFA for 30 min, permeabilized with 0.1% Triton X-100 (V900502, Sigma, USA) for 5 min, and subsequently blocked in 1% BSA (V900933-100G, Sigma, USA) diluted with PBS for 30 min. After three times washing with PBS, cells were incubated with primary anti-β-catenin (D10A8) XP antibody (8480T, Cell Signaling Technology, 1:50) overnight at 4 °C. Following another three washes in PBS, cells were incubated with anti-rabbit IgG Alexa Fluor 555 (44135, Cell Signaling Technology, IF:1:1000) for 1 h. Finally, Anti-fading Mounting Medium with DAPI (S2110, Solarbio, China) was used to visualize nuclear fluorescence. The samples and captured images were observed using a fluorescent microscope (Axio Imager.Z2, Zeiss, Germany).

RNA-sequencing (RNA-seq) analysis

We isolated MSCs from 3 weeks CKO mice ($n = 3$) and WT littermates ($n = 3$). Total RNA of non-induction MSCs in passage 3 was extracted using TRIzol reagent (15596-026, Invitrogen, USA). Libraries were prepared using TruSeq Stranded mRNA LTSample Prep Kit (Illumina, USA) and sequenced on the Illumina sequencing platform according to the manufacturer's instructions. Genes exhibiting a fold change of 2 and P -value < 0.05 were identified as significantly differentially expressed. GO and KEGG pathway enrichment of differentially expressed genes were analyzed using online tool of DAVID Bioinformatics Resources 2021²¹.

Molecular docking

The three-dimensional (3D) structures of LRP5/LRP6 were generated using Alphafold2 based on the amino acid sequence obtained from the UniProt website (www.uniprot.org/) through multiple sequence alignment. Obtained the 3D structures of ERK5 (PDB: 4ZSG) from the Protein Data Bank (PDB). The protein structure was visualized using PyMOL 2.5.32 software²⁶. We used PyMOL software to preprocess the protein structures (the removal of water molecules, hydrogen atoms, and extraneous protein regions). Subsequently, the RosettaDock software was employed to dock the target protein (ERK5) with ligand proteins (predicted LRP5 and LRP6), and calculating the docking energy within a negative value is interpreted as indicating the potential for spontaneous binding between the two proteins.

Plasmid and transfection

The single guide RNA (sgRNA) sequences for knocking out *Mapk7* using CRISPR–Cas9 were listed in Supplementary Table 2. The negative control was an empty vector plasmid (Lenti-V2). Besides, the TEY motif dominant-negative form of MAPK7 (DN-MAPK7), wild-type form of full-length MAPK7 (WT-MAPK7), as well as constitutively active form of MEK5 (CA-MEK5) were constructed as described previously²⁰. Plasmids encoding constitutive activation of Lrp6 at serine 1490 (CA-Lrp6) and mutant Lrp6 at serine 1490 (Mut-Lrp6) were constructed separately (Genecard, China). Primary MSCs or C3H10T1/2 MSCs were plated at a density of 2×10^5 cells per well in a 24-well plate overnight and transfected with plasmids using Lipofectamine 3000 (L3000-015, Invitrogen, USA). Cells were cultured in the appropriate medium to induce differentiation for various time periods.

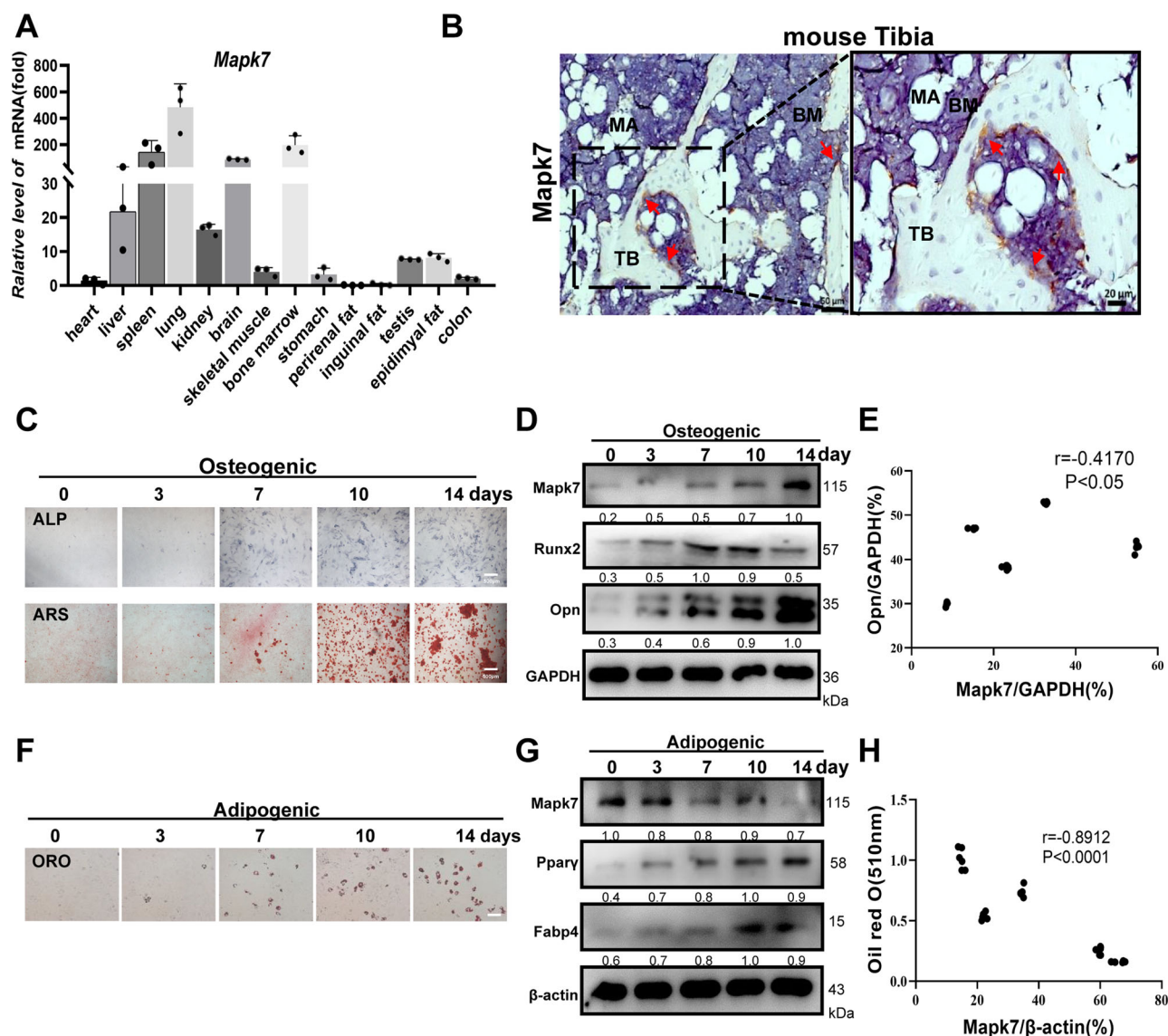


Fig. 1 | Alterations in expression of *Mapk7* during adipogenesis and osteogenesis of mMSCs. A The expression of *Mapk7* in heart, liver, spleen, lung, kidney, brain, skeletal muscle, bone marrow, stomach, perirenal fat, inguinal fat, testis, epididymal fat, and colon of 3-week-old mice. RNA expression in fat, inguinal fat, testis, epididymal fat, and colon (*GAPDH* as an internal reference gene, $n = 3$). **B** IHC results of *Mapk7* in the femur of 9-week-old mice, BM represents bone marrow, TB represents trabecular bone, MA represents bone marrow adipocytes, red arrows mark trabecular surface osteoblasts, scale bar: 500 μm (left), 20 μm (right). **C** Mouse primary MSCs derived from the femur in 3-week-old mice were stained for ALP and ARS on 0, 3, 7, 10, and 14 days of

OS induction, scale bar: 500 μm. **D** After OS induction, western blot was performed to detect the expression of *Mapk7* and osteogenesis marker genes *Runx2* and *Opn*, respectively, with *GAPDH* as an internal reference. **E** Pearson correlation analysis between *Mapk7*/GAPDH and *Opn*/GAPDH, $n = 3$. **F** Oil red O staining was performed on 0, 3, 7, 10, and 14 days of AD induction in MSCs, scale bar: 100 μm. **G** After AD induction, WB was performed to detect the expression of *Mapk7* and adipogenesis marker genes *Pparγ* and *Fabp4* in MSCs, respectively. β -actin was used as an internal reference gene. **H** Pearson correlation analysis between the relative grayscale ratio of *Mapk7*/GAPDH and OD values of Oil Red O, $n = 3$.

Statistical analysis

Results were presented as mean \pm standard deviation (SD). Besides, the error bars in the bar chart showed the corresponding SD values, and statistical analysis was conducted using GraphPad Prism 8 software. Statistical significance was determined through one-way analysis of variance, two-way analysis of variance, or Student's *t*-tests, with values of $p < 0.05$ considered statistically significant.

Results

The expression of *Mapk7* positively correlated with osteogenic differentiation of MSCs and negatively correlated with adipogenic differentiation

To explore the functions of *Mapk7* in MSCs, we first surveyed the expression of *Mapk7* in bone, fat, and other various mouse tissues. As shown in Fig. 1A,

Mapk7 was highly expressed in lung, kidney, brain, and bone marrow, and was less expressed in adipose tissue, heart, and colon, especially perirenal fat and inguinal fat. Subsequently, *Mapk7* expression was evaluated in mouse femur, and IHC results showed that *Mapk7* was highly expressed in osteoblasts and at a relatively low level in bone marrow adipocytes (Fig. 1B).

To observe the expression pattern of *Mapk7* during MSCs differentiation, we examined *Mapk7* expression during primary MSCs differentiation. As shown in Fig. 1C, ALP staining of primary MSCs was enhanced with prolonged osteogenic induction time, indicating successful differentiation. Calcium nodules appeared on day 7 of induction and increased in size and number until day 14. *Mapk7* expression elevated after osteogenic induction and peaked at day 14 (Fig. 1D). In contrast, *Mapk7* was significantly reduced during adipogenesis of MSCs (Fig. 1F and G). In addition, the expression levels of adipocyte markers, such as *Pparγ* and fatty

acid binding protein 4 (Fabp4), were elevated when primary MSCs were differentiated into adipocytes, indicating effective differentiation of adipocytes. Pearson correlation analysis revealed that *Mapk7* expression was positively correlated with osteogenic differentiation (Fig. 1E), while it was negatively correlated with the absorbance value of ORO staining during adipogenic differentiation of MSCs (Fig. 1H). Results above suggested that the expression of *Mapk7* positively correlated with the osteogenic differentiation of MSCs and negatively correlated with adipogenic differentiation.

Mapk7 positively regulated osteogenic differentiation and negatively modulated adipogenic differentiation of C3H10T1/2 MSCs

C3H10T1/2 MSCs are immortalized mesenchymal stem cells derived from mouse embryos possessing the general characteristics of MSCs^{27,28}. To clarify the influence of *Mapk7* on osteogenic (OS) and adipogenic (AD) differentiation capacities of MSCs, we employed CRISPR-Cas9 to silence *Mapk7* (Supplementary Fig. 1A). After OS induction for 3 days, we observed reduced in osteogenesis-related genes *Runx2* and *Opn*, as well as markedly diminished ALP and mineralization ability in *Mapk7*-knockout C3H10T1/2 cells (Fig. 2A–D). In contrast, *Fabp4* and *Ppar γ* , were considerably up-regulated, and lipid droplet formation was enhanced following *Mapk7* depletion in C3H10T1/2 MSCs (Fig. 2E–H). Moreover, we overexpressed *Mapk7* (OE-*Mapk7*) in C3H10T1/2 cells (Supplementary Fig. 1B) and performed OS and AD induction, respectively. Results showed the protein and mRNA levels of osteogenesis-related genes (*Runx2*, *Opn*) in OE-*Mapk7* C3H10T1/2 were significantly up-regulated after 3 days of OS induction (Fig. 2I, J). In addition, the ALP as well as mineralization ability of C3H10T1/2 cells were also significantly enhanced in OE-*Mapk7* compared with the vector group (lv242) (Fig. 2K, L). Moreover, overexpression of *Mapk7* significantly reduced protein and RNA expression of adipogenesis-related genes (*Fabp4*, *Ppar γ*) and inhibited the formation of lipid droplets in C3H10T1/2 MSCs (Fig. 2M–P). The above experiments indicated that overexpression of *Mapk7* in C3H10T1/2 MSCs enhanced osteogenic differentiation and decreased adipogenic differentiation in MSCs.

MSCs specific (*Prx1*-Cre) deletion of *Mapk7* led to decreased bone mass and increased bone marrow adipose tissue in mice

To investigate the function of *Mapk7* in MSC differentiation, we constructed *Prx1*-Cre; *Mapk7*^{lox/lox} mice (conditional knockout, CKO) by crossing *Mapk7*^{lox/lox} mice (wild type, WT) with *Prx1*-Cre mice which mainly targeted at MSCs using CRISPR-Cas9 technology and Cre-loxp system (Supplementary Fig. 2A)^{20,21}. Using specific primers, we conducted genotype identification on mouse tails (Supplementary Fig. 2B). Besides, *Prx1*-Cre; *Mapk7*^{lox/+}, *Mapk7*^{lox/lox}, and *Mapk7*^{lox/+} showed no significant differences in appearance, body length or skeletal phenotypes (Supplementary Fig. 2C and D). After extracting long bone MSCs, WB and qPCR were performed to confirm the deletion efficiency of *Mapk7* (Supplementary Fig. 2E and F). Upon birth, the CKO mice demonstrated robust survival rates and maintained normal fertility. Regardless of gender, CKO mice exhibited dwarfism and a decrease in body weight (Supplementary Fig. 2G and H). Interestingly, μ CT analysis of femurs from both control littermates (WT) and knockout littermates (CKO) postnatal was performed to compare the changes in bone-related elements in the long bones (Fig. 3A). Parameters such as BV/TV, Tb.Th, Tb.N, and Tb.Sp also indicated a substantial decrease in bone mass, indicating severe osteoporosis in CKO mice compared with 2-month-old WT littermates (Fig. 3B). Besides, the bone loss in CKO mice exhibited no sex bias (about 1:1). Furthermore, the results of Ct. Th indicated that knockout of *Mapk7* in MSCs did not significantly affect cortical bone thickness (Supplementary Fig. 2I). Furthermore, *Mapk7* CKO mice (5-month-old) exhibited a slower mineral apposition rate (MAR) and bone formation rate (BFR) compared to WT group (Fig. 3C and D). HE staining revealed a significant reduction in the number of tibial trabeculae in CKO group compared to WT group (Fig. 3E). Additionally, there is a significant decrease of Ob.S/Bs and N.Ob/B.Pm compared with CKO in expression of

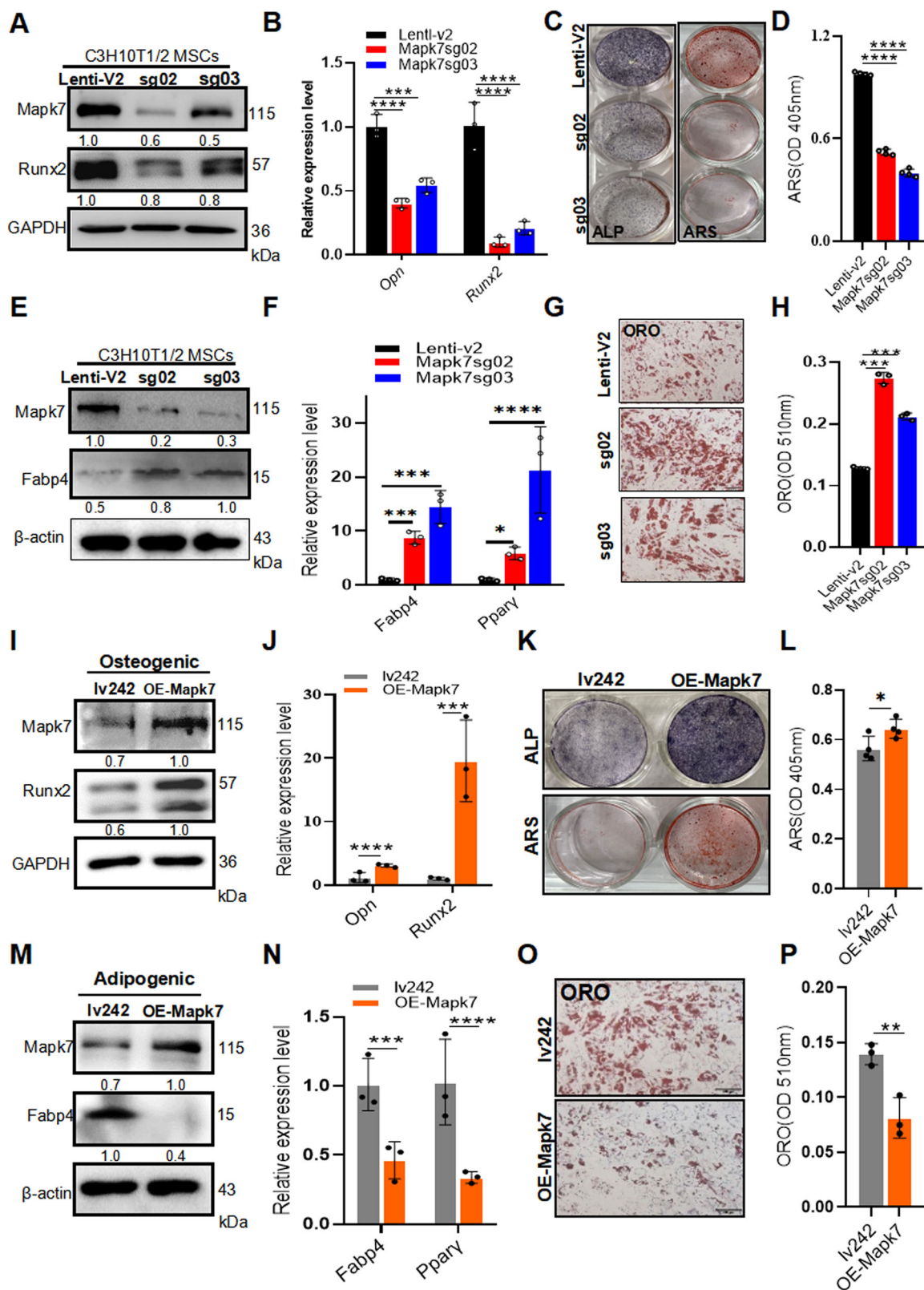
osteopontin (*Opn*), which is a marker of osteogenic cell maturation and differentiation, and *osx* (an osteogenic transcription factors) (Fig. 3F)¹⁸. Quantitative analysis of fat cells showed that the fat cell number of CKO increased compared to control WT littermates in the bone marrow cavity (Fig. 3G–I). In addition, we examined the osteoclastic activity of CKO mice. TRAP-positive osteoclastic activity was significantly enhanced in CKO littermates (Supplementary Fig. 3A and B). Subsequently, after we co-cultured MSCs with osteoclast precursor cells, the supernatant of CKO MSCs significantly promoted the multi-nuclear fusion ability of osteoclast precursor cells (Supplementary Fig. 3C). In conclusion, the skeletal manifestations of *Mapk7* CKO mice resembled the pathological phenotypes of OP with bone loss and increased bone marrow adiposity.

Mapk7 deficiency promoted adipogenic differentiation and inhibited osteogenic differentiation of primary MSCs

The accumulation of adipocytes and reduced bone formation in skeleton of *Prx1*-Cre; *Mapk7*^{lox/lox} mice prompted us to further validate the role of *Mapk7* in regulating the differentiation of primary MSCs. Firstly, the flow cytometry results demonstrated that the isolated cells from mouse compact bone were positive for mesenchymal markers CD29 and CD105, as well as the stem cell marker Sca-1, but negative for hematopoietic markers CD34 and CD45²⁹ (Fig. 4A). Further differentiation experiments revealed that primary MSCs by enzymatic digestion could readily differentiate into osteoblasts, adipocytes, and chondrocytes (Fig. 4B). Therefore, we isolated MSCs from WT and CKO mice to verify osteogenic and adipogenic potentials in vitro. Results showed that compared with WT group, the expression of *Runx2* and *Opn* of CKO MSCs was down-regulated (Fig. 4C, D). Likewise, ALP and ARS staining decreased in CKO MSCs (Fig. 4E), which indicated that *Mapk7* knockdown resulted in reduced osteogenesis of MSCs. Next, we investigated the role of *Mapk7* in adipogenesis of MSCs. Consistently, expression of adipogenesis genes (*Fabp4* and *Ppar γ*) and ORO staining were both significantly enhanced in CKO compared with WT MSCs (Fig. 4F–H), indicating that *Mapk7* deletion enhanced adipogenesis of MSCs. Collectively, above results further clarified that *Mapk7* regulated the balance of fate commitment of MSCs by inhibiting adipogenesis and enhancing osteogenesis.

Wnt/ β -catenin signaling was significantly reduced after *Mapk7* deletion in MSCs

To explore the underlying mechanism of *Mapk7* in the regulation of osteoblast-adipocyte lineage transition in MSCs, we extracted RNA from the same generation of non-induction MSCs in littermate WT and CKO mice for RNA-seq, and results showed that 151 genes were up-regulated and 376 genes were down-regulated in CKO compared with WT (Fig. 5A), where down-regulated genes were mainly enriched in extracellular matrix receptor interaction, cytoskeleton regulation, PI3K-Akt signaling and Wnt pathways (Fig. 5B). In recent years, numerous studies have shown that MAPK family acted as important intermediate signaling molecules to regulate Wnt signaling activity which regulates cell fate determination and tissue homeostasis^{10,30}. Since Wnt signaling consists of both β -catenin-dependent and β -catenin-independent pathways, previous researches have indicated that ERK could potentiate non-canonical Wnt cascades, such as Wnt/PCP signaling²⁰. However, Nagano et al. confirmed that enhancing Erk phosphorylation could activate classical Wnt signaling to regulate bone formation in the appendicular skeleton¹⁰. Gene set enrichment analysis (GSEA) results showed that Wnt signaling was significantly enriched in *Mapk7*-deficient MSCs (Fig. 5C). Subsequently, we examined the expression of active (non-phospho-) β -catenin, an effector molecule of classical Wnt pathway. Immunofluorescence results showed active (non-phospho-) β -catenin decreased in CKO tibia compared to WT tibia (3-weeks-old mice) (Fig. 5D). Besides, translocation of β -catenin into nucleus was reduced in CKO MSCs (Fig. 5E). In addition, active β -catenin were significantly reduced in CKO MSCs compared to WT in both total protein extract and nuclear protein extract (Fig. 5F), and deletion of *Mapk7* resulted a significant decrease in the



expression of canonical Wnt target genes (*C-Myc* and *Cyclin D1*) (Fig. 5G), accompanied by an elevation in active β -catenin, which was also consistent with the reduced of *Runx2*, an osteogenic-related target factor of canonical Wnt signaling^{30,31}. The above results suggested that *Mapk7* deletion in MSCs inhibited Wnt/ β -catenin signaling activity.

Wnt/ β -catenin pathway activator, CHIR-99021 rescued *Mapk7* knockdown-induced attenuated osteogenesis and increased adipogenesis in MSCs in vitro

To further confirm that Wnt/ β -catenin signaling was a critical pathway for *Mapk7*-mediated differentiation of MSCs, we introduced an activator for classical Wnt/ β -catenin signaling, CHIR-99021²⁷. After OS differentiation,

Fig. 2 | Regulatory role of Mapk7 in osteogenic and adipogenic differentiation of C3H10T1/2 MSCs. **A** Proteins were collected after OS differentiation for 3 days to detect the expression of Mapk7 and osteogenic marker gene *Runx2*, following knocking out of *Mapk7* in C3H10T1/2 MSCs, Lenti-V2 was the control group, with *GAPDH* as an internal reference gene. **B** After knocking out of *Mapk7* in C3H10T1/2, RNA was collected after OS differentiation for 3 days to detect the RNA level of Mapk7 and osteogenic marker genes *Runx2* and *Opn*, with *GAPDH* as an internal reference gene, $n = 3$, $^{***}p < 0.005$, $^{****}p < 0.001$. **C** Following OS differentiation, ALP and ARS staining were performed, respectively. **D** ARS nodules were solubilized with DMSO to detect OD values (405 nm), $n = 3$, $^{****}p < 0.001$. **E** After AD differentiation for 3 days, proteins were collected to detect the expression of Mapk7 and adipogenesis-related gene *Fabp4*, with β -actin as an internal reference gene. **F** After AD differentiation for 3 days, RNA was collected to detect the expression of *Mapk7* and adipogenesis marker genes (*Fabp4* and *Ppar γ*), and β -actin was used as an internal reference gene, $n = 3$, $^{***}p < 0.005$, $^{****}p < 0.001$. **G** ORO staining of AD differentiation, scale bars: 100 μ m. **H** Lipid droplets were solubilized with isopropanol to detect the OD value (510 nm), $n = 3$, $^{***}p < 0.005$. **I** After OS

differentiation, proteins were collected for western blot to detect protein expression of Mapk7 and osteogenic marker genes *Runx2* and *Opn*, with *GAPDH* as an internal reference gene. **J** After OS differentiation was performed for 3 days, RNA was collected for qPCR to detect the expression levels of *Mapk7* and osteogenic marker genes (*Runx2*, *Opn* and *Alpl*), with *GAPDH* as internal reference gene, $n = 3$, $^{***}p < 0.005$, $^{****}p < 0.001$. **K** ALP and ARS staining. **L** ARS positive nodules were solubilized with DMSO, and OD values (405 nm) were detected, $n = 3$, $^{*}p < 0.05$. **M** After AD differentiation was performed for 3 days, the expression of Mapk7 and adipogenesis marker protein (*Ppar γ* and *Fabp4*) were detected, β -actin was used as an internal control. **N** After overexpression of *Mapk7* in C3H10T1/2, AD differentiation was performed for 3 days, RNA was collected for qPCR, and expression of Mapk7 and adipogenesis marker genes (*Fabp4* and *Ppar γ*) were detected, β -actin as an internal reference gene, $n = 3$, $^{***}p < 0.005$, $^{****}p < 0.001$. **O** After AD differentiation 14 days, ORO staining was performed, scale bar: 500 μ m. **P** Lipid droplets were solubilized with isopropanol, and OD value (510 nm) was detected, $n = 3$, $^{**}p < 0.01$.

calcium nodules in CKO MSCs were notably increased after CHIR-99021 (10 μ M) treatment compared with the DMSO group (Fig. 6A and B). In contrast, ORO results also showed that the adipogenic capacity of CKO MSCs was inhibited by CHIR-99021 (Fig. 6C and D). Besides, *Runx2* was significantly up-regulated after the CHIR-99021 application (Fig. 6E). At the same time, expression of active β -catenin in CKO MSCs did appear to be down-regulated and increased after the CHIR-99021 application (Fig. 6E), reflecting that CHIR-99021 could indeed activate Wnt/ β -catenin signaling. Conversely, CHIR-99021 decreased *Fabp4* expression in CKO MSCs (Fig. 6G). Moreover, CHIR-99021 activation of Wnt signaling rescued the expression of osteogenic genes (*Runx2*, *Alpl*) in CKO MSCs (Fig. 6F). Likewise, the levels of adipogenesis-related genes (*Cebpa*, *Fabp4*) were both partially rescued in CKO group after activation of Wnt/ β -catenin signaling (Fig. 6H). Taken together, CHIR-99021 ameliorated the imbalance of osteogenic and adipogenic differentiation in MSCs caused by *Mapk7* deletion through activation of Wnt/ β -catenin pathway, which further identified the indispensable role of Wnt/ β -catenin signaling in *Mapk7*-deficiency mediated imbalance between osteogenesis and adipogenesis of MSCs.

Mapk7 enhanced osteogenesis and inhibited adipogenesis of MSCs through phosphorylation of Lrp6 at Ser1490

MAPK7 is one of the kinases of the MAPK family which phosphorylates a range of substrates essential for osteogenesis²⁸. Therefore, we co-transfected MEK5 constitutive activated (CA-MEK5), wild-type MAPK7-WT and MAPK7 dominant negative plasmids (DN-MAPK7)²⁰ in C3H10T1/2 to investigate whether Mapk7 regulated osteogenic and adipogenic differentiation in MSCs through phosphorylation function (Fig. 7A). After MAPK7 was persistently activated by MEK5, osteogenic genes were significantly up-regulated and adipogenic genes were significantly down-regulated, while the expression of osteogenesis and adipogenesis-related genes were all reverted after MAPK7 mutation (Fig. 7B and C), indicating that phosphorylation function of Mapk7 was involved in regulating osteogenic and adipogenic differentiation in MSCs.

Since *Mapk7* deletion resulted in reduced nucleation of β -catenin, we further investigated whether Mapk7 regulated the activity of key molecules in Wnt/ β -catenin signaling. It is known that in the absence of Wnt stimulation, β -catenin can be constitutively phosphorylated by glycogen synthase kinase-3 β (Gsk3 β), leading to ubiquitination and proteasome-dependent degradation of β -catenin³². Furthermore, members of the LRP family, including LRP4, LRP5, and LRP6, are all single-pass trans-membrane proteins containing multiple phosphorylation sites^{32–34}. Considering that LRP4 facilitated sclerostin-mediated inhibition of Wnt signaling, while LRP5/6, in conjunction with Frizzled receptors regulated β -catenin stability, and functional mutations in LRP6 were associated with the occurrence of OP^{32–34}, we conducted molecular docking between MAPK7 (ERK5) and LRP5/ LRP6, respectively. The results revealed the docking energy between

LRP6 and ERK5 was -7.9 kJ/mol, which was lower than the minimum docking energy observed for LRP5 (Supplementary Fig. 4A). This suggested a stronger binding potential between ERK5 and LRP6. Furthermore, the phosphorylation levels of Lrp6 and Gsk3 β were significantly decreased after MAPK7 mutation (Fig. 7D). Meanwhile, p-Lrp6 levels in CKO tibiae were also significantly lower than in WT group via IHC (Fig. 7E). Previous study has shown that ERK directly induced Gsk3 β T43 phosphorylation, which in turn regulated β -catenin activity³³, so we need to clarify whether Gsk3 β was involved in the regulatory process in our system. Therefore, to verify whether Mapk7 phosphorylated Gsk3 β /Lrp6 by binding them, we found that p-Mapk7 could co-precipitate with Lrp6 by IP (Fig. 7F), while there was no co-precipitation with Gsk3 β (Supplementary Fig. 5A), indicating that p-Mapk7 interacted with Lrp6. And as the phosphorylation level of Mapk7 increased, the phosphorylation level of Lrp6 at Ser1490 also gradually increased (Fig. 7G).

Given that the phosphorylation level of Lrp6 at Ser1490 was activated by Mapk7, therefore, we further investigated whether the phosphorylation of Lrp6 at Ser1490 by Mapk7 was involved in MSCs osteogenic and adipogenic differentiation. Activation of classical Wnt/ β -catenin pathway was initiated by the binding of Wnt proteins to cell surface receptors¹¹, we utilized a co-culture system of L-Wnt3A and MSCs to activate Wnt/ β -catenin signaling in MSCs. Besides, the transfection of CA-Lrp6 under activation of Wnt3a significantly enhanced the level of p-Lrp6 (Ser1490) in CKO MSCs (Fig. 7H). Moreover, activation of Lrp6 at Ser1490 significantly enhanced the level of osteogenic markers (*Opn* and *Runx2*) in CKO MSCs (Fig. 7H). As expected, ARS staining was also consistent with WB (Fig. 7I, J). Similarly, under AD differentiation conditions, activation of Lrp6 at Ser1490 significantly reduced the level of adipogenesis protein (*Ppar γ* and *Fabp4*) and improved the accumulation of lipid droplets in CKO MSCs (Fig. 7K–M). In conclusion, the results above suggested that the activating effect of Mapk7 on Lrp6 Ser1490 was essential for enhancing osteogenesis and inhibiting adipogenesis of MSCs.

Discussion

In this study, we initially demonstrated that deletion of *Mapk7* in MSCs led to a significant loss in bone mass accompanied by an increase in bone marrow adiposity. Furthermore, overexpression and deletion experiments showed that *Mapk7* played a crucial role in promoting osteogenic differentiation in MSCs while simultaneously inhibiting adipogenesis. Mechanistically, the findings revealed that Mapk7 could phosphorylate Ser1490 of LRP6, promoting the nuclear translocation of β -catenin, and thereby regulating bone mass and bone marrow adiposity. The findings further broaden the understanding of the crosstalk between the MAPK family member, Mapk7, and Wnt/ β -catenin signaling in the differentiation of MSCs.

MAPK7, through its phosphorylation function, regulated cellular functions in a wide variety of tissues^{35,36}. The present findings

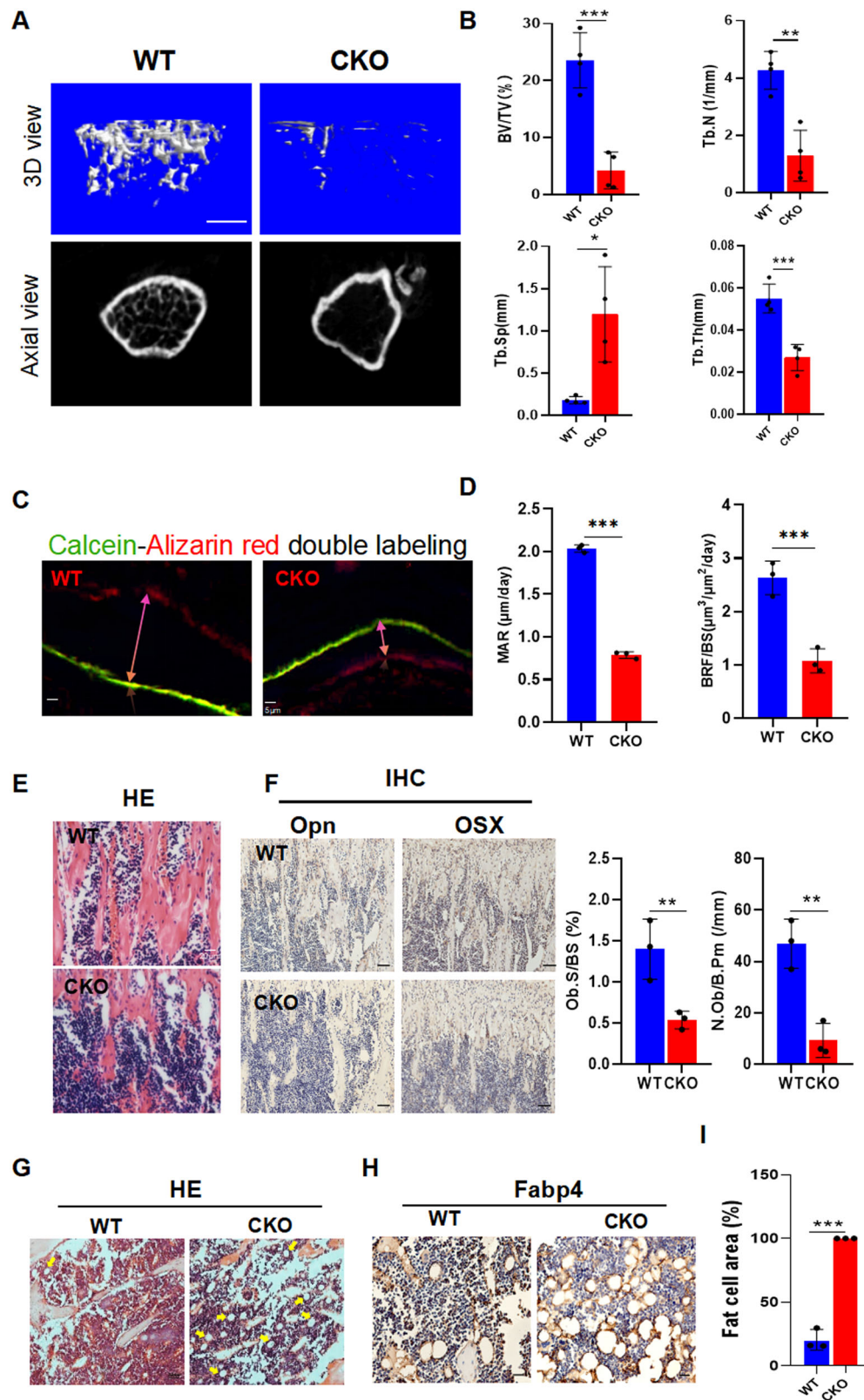


Fig. 3 | Effect of MSCs-specific knockout of *Mapk7* on bone mass and bone marrow adiposity in mice. **A** and **B** μ CT maps (**A**) and quantitative results (**B**) of scan-related bone parameters in 2-month-old *Mapk7* knockout mice and WT littermates regards of gender, $n = 4$, * $p < 0.05$, ** $p < 0.01$, *** $p < 0.005$, scale bar: 2 mm. **C** Representative image of double labeling with Calcein-Alizarin red from in cancellous bone regions from proximal femur sections in 9-week-old mice, scale bar: 5 μm . **D** The dynamic bone histomorphometry indexes of 9-week-old mice, including MAR and BFR/BS, $n = 3$, *** $p < 0.005$. **E** HE staining of tibiae of 3-week-old

mouse, scale bar: 20 μm . **F** IHC results of osteogenic marker protein Opn and Osx in tibiae of 3-week-old mice and the quantitative of bone surface covered by osteoblasts Ob.S/BS (%), the number of osteoblasts per mm endocortical bone surface (N. Ob/B.Pm/mm), $n = 3$, ** $p < 0.01$, scale bar: 50 μm . **G** HE staining of tibiae from 2-month-old mice, yellow arrows show adipocytes, scale bar: 20 μm . **H** and **I** IHC of adipose tissue marker protein Fabp4 and relative area of adipocytes in the distal marrow per tissue area ($n = 3$); *** $p < 0.005$, scale bar: 50 μm .

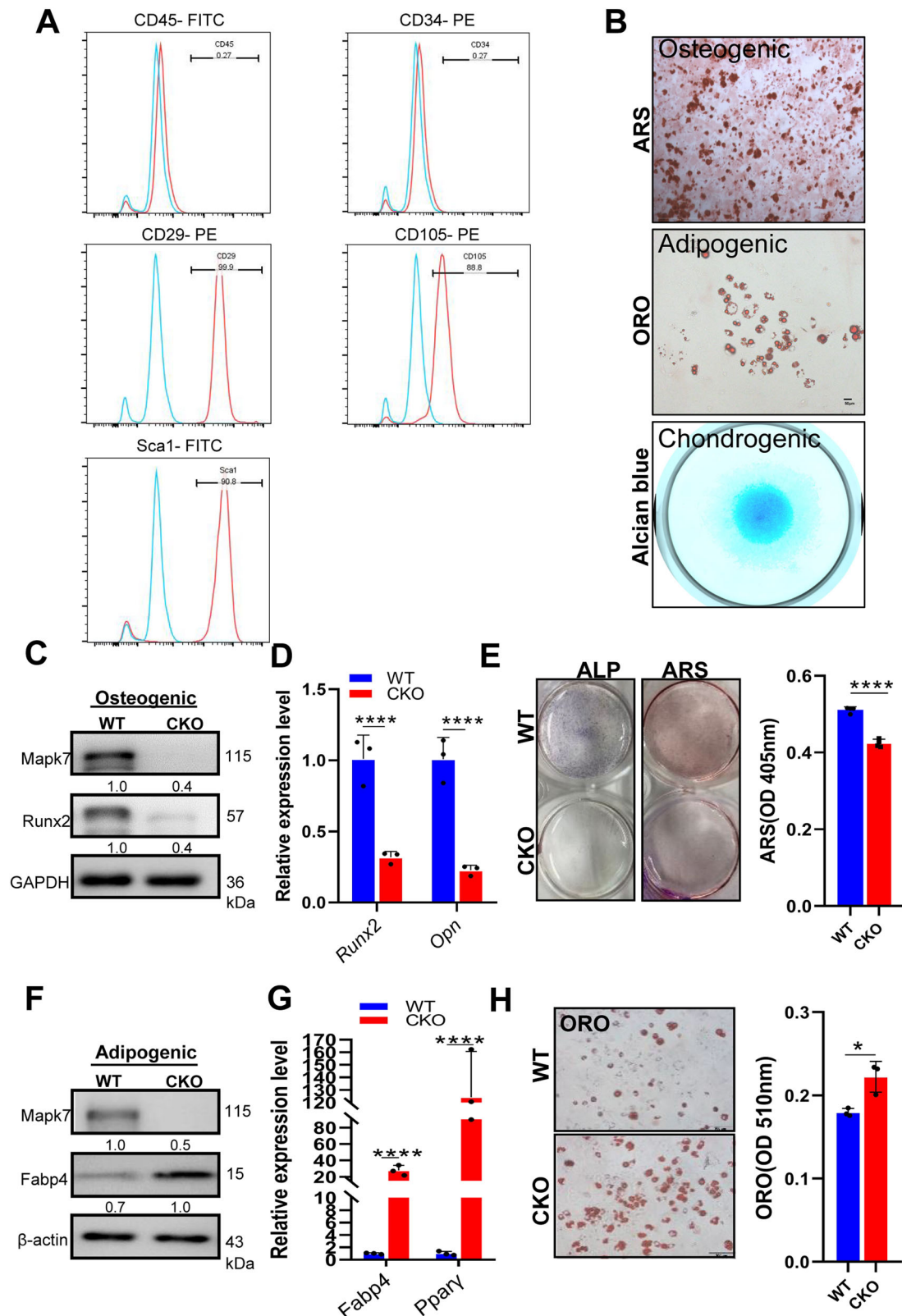


Fig. 4 | Osteogenic and adipogenic differentiation of MSCs derived from *Mapk7* CKO mice. **A** Immunophenotypic characterization of CD45, CD34, CD29, Sca1 and CD105. **B** Osteogenic, adipogenic, and chondrogenic differentiation assays of mouse primary MSCs derived from femur and tibia in 3-week-old mice, scale bar: 650 μ m (upper); 50 μ m (middle). **C** The expression of Mapk7, osteogenic marker protein (Runx2) was detected 3 days after OS induction of primary MSCs in passage 3 derived from 3-week-old WT and littermate CKO mice. **D** mRNA levels of *Runx2*, *Opn*, $n = 3$,

**** $p < 0.0001$. **E** Results of ALP and ARS staining in MSCs in passage 3 after 7 and 14 days of OS induction, $n = 3$, **** $p < 0.0001$. **F** Expression of Mapk7, adipogenic marker protein Fabp4 was detected 3 days of primary MSCs after AD induction. **G** mRNA levels of *Fabp4* and *Pparg* were detected 3 days of primary MSCs after AD induction, $n = 3$, **** $p < 0.0001$. **H** Results of ORO staining and quantification at 14 days of AD induction of primary MSCs at passage 3 derived from WT and littermate CKO mice, scale bar: 50 μ m, $n = 3$, * $p < 0.05$.

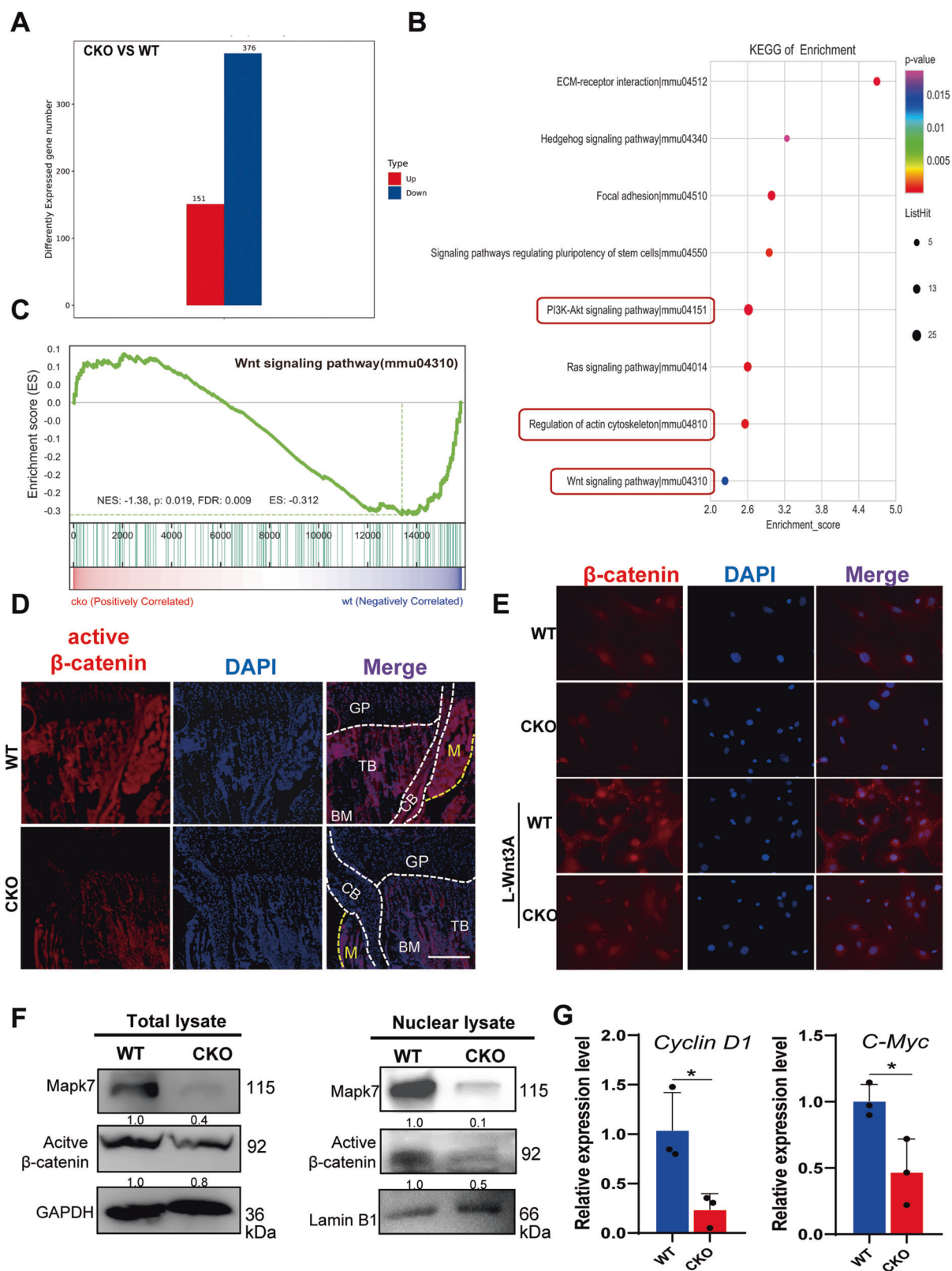
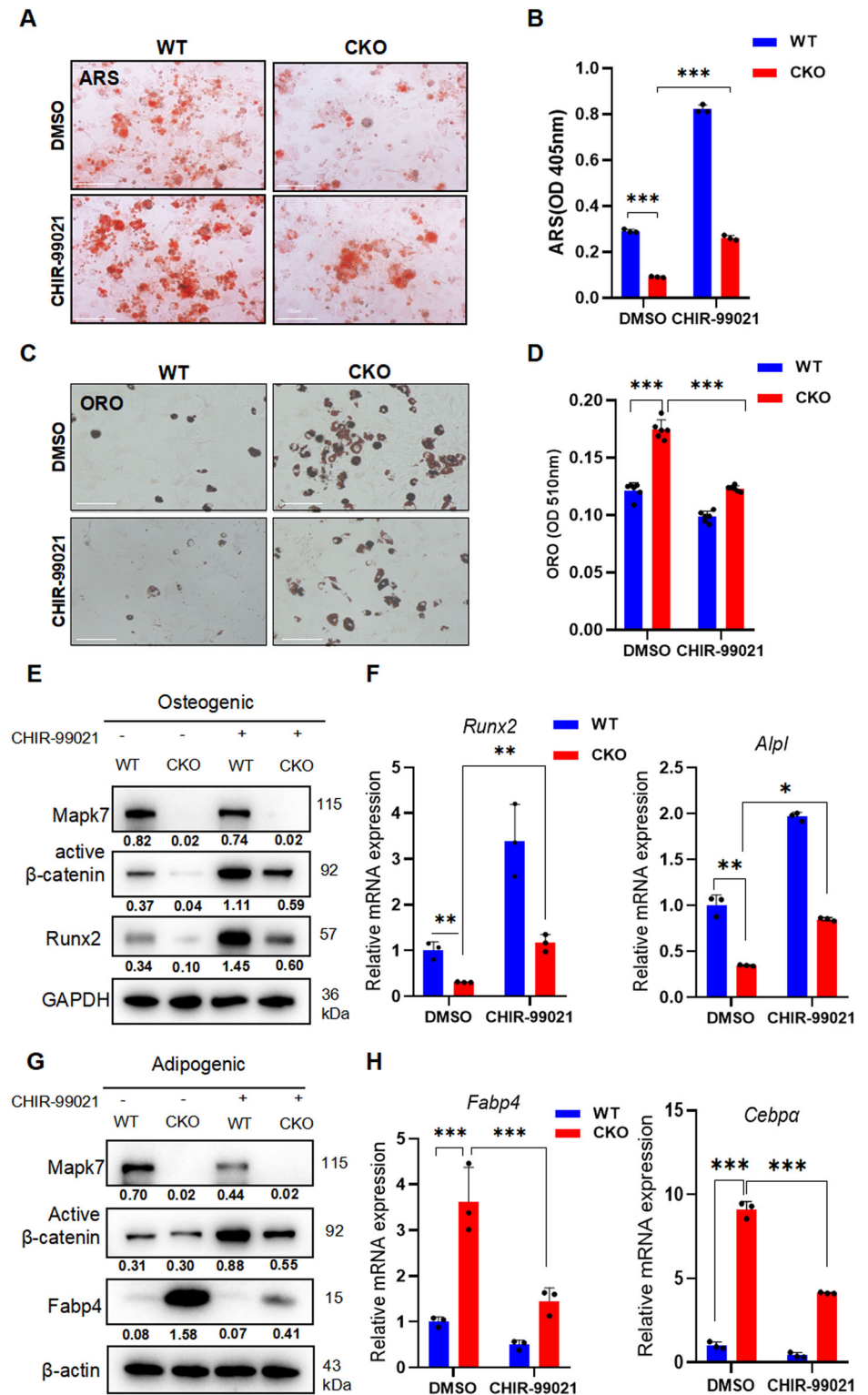


Fig. 5 | Deletion of *Mapk7* in MSCs inhibited Wnt/ β -catenin pathway.

A Differentially expressed genes after RNA-seq of RNA from primary MSCs isolated from 3-week-old. WT and littermate CKO mice at passage 3. **B** and **C** Results of KEGG enrichment (**B**) and GSEA analysis of differential genes (**C**). **D** Representing active β -catenin IF images of tibia at 3-weeks old mice. Dotted lines mark different locations, BM bone marrow, TB trabecular bone, M muscle, CB cortical bone, GP growth plate; scale bars: 100 μ m. **E** IF results of total β -catenin in MSCs at passage 4

co-cultured with or without L-Wnt3A cells via a trans-well device, scale bar: 50 μ m. **F** Detection of *Mapk7* and classical Wnt pathway effector molecular activity, active β -catenin expression in total protein extracts and nuclear protein extracts from mouse MSCs at passage 4, GAPDH and Lamin B1 were used as internal reference genes for total and nuclear proteins, respectively. **G** Detection of the RNA level of β -catenin target genes *C-Myc* and *CyclinD1*, with *GAPDH* as an internal reference gene, $n = 3$, $p < 0.05$.

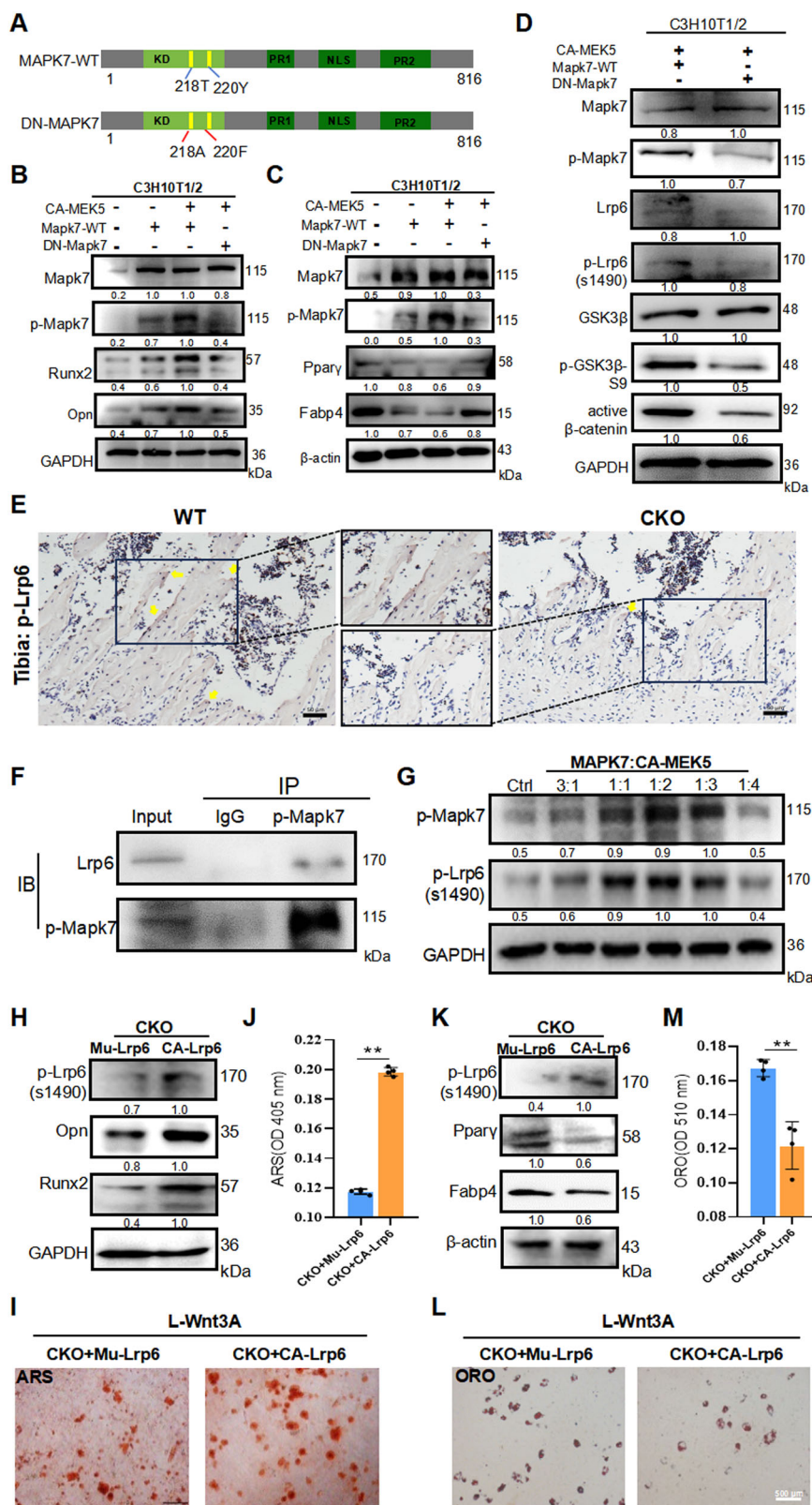
Fig. 6 | CHIR-99021, an activator of Wnt/ β -catenin pathway ameliorated the imbalance between osteogenic and adipogenic differentiation in MSCs caused by *Mapk7* deletion. A ARS staining for CHIR-99021 (10 μ M) treatment to primary MSCs at passage 4 after OS induction for 14 days, scale bar: 150 μ m. **B** Quantitative of ARS staining, $n = 3$, *** $p < 0.005$. **C** ORO staining for CHIR-99021 (10 μ M) treatment to primary MSCs at passage 4 after OS induction, scale bar: 200 μ m. **D** Quantitative of ORO staining, $n = 3$, *** $p < 0.005$. **E** Protein expression of Mapk7, osteogenesis-related genes (*Runx2*), and β -catenin was detected after OS induction of primary MSCs for 3 days with CHIR-99021 (10 μ M) treatment. **F** Application of CHIR-99021 (10 μ M) to MSCs at passage 4 after OS induction for 3 days, qPCR was performed to detect the levels of osteogenesis-related genes (*Runx2*, *Alpl*), $n = 3$, * $p < 0.05$; ** $p < 0.01$. **G** Primary MSCs at passage 4 of WT/CKO mice were treated with CHIR-99021 (10 μ M) for 3 days after AD induction, and Western blot was performed to detect the expression of Mapk7, adipogenesis-related gene (*Fabp4*) and active β -catenin, β -actin was used as an internal control. **H** Adipogenesis of primary MSCs at passage 4 was induced for 3 days along with CHIR-99021 (10 μ M) treatment, then qPCR was performed to detect the mRNA levels of lipid formation-related genes (*Fabp4*, *Cebpa*), $n = 3$, *** $p < 0.005$.



underscored the importance of the phosphorylation function of MAPK7 (ERK5) phosphorylation in promoting osteogenic differentiation while inhibiting adipogenic differentiation in MSCs. Adam et al.³⁷ demonstrated that knockdown of *ERK5* or the use of ERK5 inhibitor XMD8-92 to suppress ERK5 phosphorylation inhibited osteogenic differentiation in human MSCs, aligning with our findings and further verifying the crucial regulatory role of Mapk7 phosphorylation in MSC osteogenic differentiation. Prior research has shown that MSCs could be traced using markers such as *Prx1*, *Dermo1*, *LepR*, and *Nestin*^{38–40}. Our study revealed

that the ablation of *Mapk7* in MSCs reduced bone mass in mouse long bones, with further confirmation in C3H10T1/2 MSCs that the lack of *Mapk7* inhibited osteogenic differentiation. However, the deletion of *Mapk7* in *LepR*⁺ MSCs enhanced osteogenic differentiation in MSCs⁴¹. One explanation was that *Prx1* was expressed predominantly in mesenchymal progenitors during embryonic development. This suggested that *Prx1*⁺ MSCs might be present much earlier in development than *LepR*⁺ MSCs. *LepR* might thus represent an MSC population that was more associated with osteogenic and osteocytic generative activity.

Fig. 7 | Mapk7 regulated osteogenic and adipogenic differentiation of MSCs through Lrp6/ β -catenin signaling. **A** Schematic illustration of MAPK7-WT and the DN-MAPK7 mutation. **B** and **C** Expression of Mapk7, p-Mapk7, osteogenesis-related genes (Ppar γ , Fabp4) were detected after 3 days of OS (**B**) and AD (**C**) induction in C3H10T1/2 cells transfected with the corresponding plasmid, respectively, and GAPDH and β -actin were used as internal reference genes. **D** The expression of key molecules of Wnt/ β -catenin signaling in C3H10T1/2 cells after transfected with the corresponding plasmid, and GAPDH was used as an internal reference gene. **E** p-Lrp6 staining of 2-month-old mouse tibiae using IHC, yellow arrowheads mark the positive region of p-Lrp6 expression. scale bar: 50 μ m. **F** IP assay of Lrp6 and p-Mapk7 interactions in C3H10T1/2 cells. **G** C3H10T1/2 MSCs were transfected with different ratios of MAPK7-WT: CA-MEK5 to detect the expression of p-Mapk7, p-Lrp6 (Ser1490), and GAPDH as an internal reference gene. **H** Primary MSCs at passage 4 were transfected with constitutive activation Lrp6 at Ser1490 plasmid (CA-Lrp6) and inactivation mutation plasmid (Mu-Lrp6) and were co-cultured with L-Wnt3A cells, whose p-Lrp6 (Ser1490)/ osteogenesis-related genes (Opn and Runx2) were detected after 3 days of osteogenic induction. **I** ARS staining of primary passage 4 MSCs which were co-cultured with L-Wnt3A cells under the condition of OS induction for 14 days, scale bar: 500 μ m. **J** Quantitative results of ARS staining, $n = 3$, $^{**}p < 0.01$. **K** Expression levels of p-Lrp6 (Ser1490), Lrp6, and adipogenesis-related genes (Ppar γ and Fabp4) were tested in passage 4 MSCs, which were transfected with CA-Lrp6 and Mu-Lrp6, co-cultured with L-Wnt3A cells after 3 days of AD induction. **L** ORO staining after 14 days of AD induction under co-culture conditions of passage 4 MSCs and L-Wnt3A, scale bar: 500 μ m. **M** Quantitative results of ORO, $n = 3$, $^{**}p < 0.01$.



This also suggested that Mapk7 exhibited functional heterogeneity in different cell types. Furthermore, in the physiological microenvironment of bone marrow, bone formation increased while fat accumulation decreased³⁵. In our study, *Prx1*-Cre; *Mapk7*^{fllox/fllox} mice exhibited decreased osteogenesis accompanied by abnormally increased adipose tissue in the marrow. Our in vitro gain- and loss-of-function studies also

confirmed that Mapk7 inhibited adipogenic differentiation in MSCs. Similarly, the deletion of *Mapk7* in *LepR*⁺ MSCs resulted in abnormal increases in bone marrow adiposity⁴¹. *LepR* was primarily a marker of MSCs in adults, whereas *Prx1* was pressed largely by MSCs during embryonic development^{35,36}, suggesting that the absence of *Mapk7* at different developmental stages led to increased marrow adipose tissue.

The study showed that *Mapk7* deletion in MSCs resulted in short stature at birth, consistent with previous research²⁸. The elongation of the limbs and long bones occurs through endochondral ossification. Researchers have found that specific knockout of *Mapk7* in chondrocytes (*Col2al-Cre; Mapk7^{fllox/fllox}*) inhibited hypertrophic differentiation of growth plate chondrocytes in mice⁴². Since chondrocytes originate from mesenchymal cells⁴³, the short-stature phenotype observed in CKO mice in this study might have been due to the absence of *Mapk7* in MSCs. Additionally, MSC-mediated bone formation and osteoclast-mediated bone resorption jointly maintain bone homeostasis. Interestingly, the CKO mice in the study exhibited enhanced osteoclast activity in long bones. Previous reports have shown that the deletion of *Mapk7* in osteoclast lineage precursors led to increased osteoclast activity, resulting in increased bone resorption and reduced bone mass in postnatal *Nkx3.1-Cre; Mapk7^{fllox/fllox}* mice¹³. However, *Prx1* was not a marker of osteoclast lineage precursors³⁹. Therefore, we co-cultured bone marrow-derived macrophages (BMMs) with MSCs and found that BMMs co-cultured with CKO MSCs exhibited enhanced osteoclast activity. Previous studies have reported that MSCs acted as secretory cells influencing the activities of surrounding cells, with MSCs-derived extracellular vesicles (MSC-EVs) loaded with microRNAs regulating osteoclast activity⁴⁴. This suggested that CKO MSCs might affect the osteoclast activity of BMMs through paracrine signaling. Another possible explanation is that, following *Mapk7* knockout, the tendency of MSCs toward adipogenic differentiation promoted their ability to enhance osteoclast activity in BMMs. Recent research by Fan et al. indicated that in the absence of *Pth1r* in MSCs, bone marrow adipocytes served as one of the sources of receptor activators of nuclear factor- κ B ligand (RANKL), affecting osteoclast activity⁴³. Therefore, elucidation of the differentiation potential of MSCs toward adipocytes following *Mapk7* deletion and its impact on osteoclast-inducing factors such as RANKL in regulating osteoclast activity will be an intriguing area for further research. In conclusion, our findings suggested that *Mapk7* regulated cell differentiation and fate across different cell types, to collectively maintain bone homeostasis.

MAPK7, as a member of the conserved MAPK family, transmits downstream signals through the phosphorylation of various substrates^{20,45}. ERK5, rather than ERK1/2, phosphorylated FAK at Ser910 to modulate cell migration⁴⁶. The findings of the present study further extended the known functions of MAPK7 to include the promotion of β -catenin nuclear translocation in MSCs. It was shown that the osteogenic and adipogenic phenotypes of MSCs were dependent on *Mapk7* phosphorylation of Lrp6 at Ser1490, and the activation of TEY motif in the kinase domain played a crucial role in this process. In addition, another family member of ERK, ERK1/2, has been previously demonstrated to bind to LRP6 to regulate Wnt/ β -catenin signaling activity, serving as a regulatory factor for MSC differentiation although the site of interaction between ERK1/2 and LRP6 was not investigated^{3,10}. However, the TEY motif in the kinase domain was relatively conserved in the MAPK family. Therefore, we speculated that LRP6 might be a common substrate of MAPK family members with the TEY motif. Besides, we have previously shown that *Mapk7* participates in vertebral development by regulating MEF2C/PTEN/AKT signaling to modulate chondrocyte hypertrophic differentiation⁴³. Therefore, considering that MEF2C represents as a classic substrate in the MAPK cascade^{15,47}, we overexpressed MEF2C to assess its potential in reversing the imbalance between osteogenic and adipogenic differentiation in MSCs due to *Mapk7* deficiency. Nevertheless, our findings indicated that MEF2C was unable to compensate for changes resulting from the absence of *Mapk7* (Supplementary Fig. 6A and B), hinting at the existence of *Mapk7* functional heterogeneity across different cell types.

In all, our study established a connection between MSC fate decisions and protein kinases, demonstrating that *Mapk7* was a vital regulator of MSC differentiation through Lrp6 phosphorylation. Clarifying the relationship between *Mapk7* and the Wnt/ β -catenin pathway may

provide new insights for future research on targeted therapy for diseases associated with MSC differentiation, such as OP. Due to its expression in multiple tissues and the significant roles of MAPK7, a systemic treatment that targets MAPK7 directly would pose considerable risks. It has been reported that transplantation of genetically modified MSCs stimulated osteogenic differentiation and new bone formation to suppress age-related OP-like phenotypes⁴⁸. Besides, clinical trials using MSC injection for the treatment of various diseases, such as osteoarthritis, are currently underway⁴⁹. Therefore, our findings may provide therapeutic targets for OP and preliminary laboratory data for future clinical treatment of severe OP, for instance, the use of intramedullary injections of genetically modified MSCs.

Data availability

All data of RNA-seq have been deposited to the NCBI GeneExpression Omnibus (GSE255596). The source data behind the graphs in the paper was exhibited in Supplementary Data 1. Uncropped and unedited blot images were exhibited in Supplementary Fig. 7. Plasmids first constructed in this study have been deposited to the Addgene (ID:234364 and 234365).

Received: 4 April 2024; Accepted: 18 February 2025;

Published online: 26 February 2025

References

- Deng, P. et al. Loss of KDM4B exacerbates bone-fat imbalance and mesenchymal stromal cell exhaustion in skeletal aging. *Cell Stem Cell* **28**, 1057–1073 (2021).
- Zhang, L. et al. Hedgehog signaling controls bone homeostasis by regulating osteogenic/adipogenic fate of skeletal stem/progenitor cells in mice. *J. Bone Miner. Res.* **37**, 559–576 (2022).
- Tian, L. et al. A novel Sprouty4-ERK1/2-Wnt/ β -catenin regulatory loop in marrow stromal progenitor cells controls osteogenic and adipogenic differentiation. *Metabolism* **105**, 154189 (2020).
- Lee, K. S. et al. Extracellular vesicles from adipose tissue-derived stem cells alleviate osteoporosis through osteoprotegerin and miR-21-5p. *J. Extracell. Vesicles* **10**, e12152 (2021).
- Liu, Z. Z. et al. Autophagy receptor OPTN (optineurin) regulates mesenchymal stem cell fate and bone-fat balance during aging by clearing FAPB3. *Autophagy* **17**, 2766–2782 (2021).
- Olona, A. et al. Adipoclast: a multinucleated fat-eating macrophage. *BMC Biol.* **19**, 246 (2021).
- Chen, Q. et al. Fate decision of mesenchymal stem cells: adipocytes or osteoblasts? *Cell Death Differ.* **23**, 1128–1139 (2016).
- Basisty, N. et al. A proteomic atlas of senescence-associated secretomes for aging biomarker development. *PLoS Biol.* **18**, e3000599 (2020).
- During, A. Osteoporosis: a role for lipids. *Biochimie* **178**, 49–55 (2020).
- Nagano, K. et al. R-spondin 3 deletion induces Erk phosphorylation to enhance Wnt signaling and promote bone formation in the appendicular skeleton. *Elife* **11**, e84171 (2022).
- Tian, L. et al. A novel Sprouty4-ERK1/2-Wnt/ β -catenin regulatory loop in marrow stromal progenitor cells controls osteogenic and adipogenic differentiation. *Metabolism* **105**, 154189 (2020).
- Cong, Q. et al. p38a MAPK regulates lineage commitment and OPG synthesis of bone marrow stromal cells to prevent bone loss under physiological and pathological conditions. *Stem Cell Rep.* **6**, 566–578 (2016).
- Loveridge, C. J. et al. Analysis of *Nkx3.1: Cre-driven Erk5* deletion reveals a profound spinal deformity which is linked to increased osteoclast activity. *Sci. Rep.* **7**, 13241 (2017).

14. Schroyer, A. L., Stimes, N. W., Abi Saab, W. F. & Chadee, D. N. MLK3 phosphorylation by ERK1/2 is required for oxidative stress-induced invasion of colorectal cancer cells. *Oncogene* **37**, 1031–1040 (2018).
15. Paudel, R., Fusi, L. & Schmidt, M. The MEK5/ERK5 pathway in health and disease. *Int. J. Mol. Sci.* **22**, 7594 (2021).
16. Zhou, T. et al. Mutant MAPK7-Induced Idiopathic Scoliosis is Linked to Impaired Osteogenesis. *Cell. Physiol. Biochem.* **48**, 880–890 (2018).
17. Zhao, X. et al. ZBP1 (DAI/DLM-1) promotes osteogenic differentiation while inhibiting adipogenic differentiation in mesenchymal stem cells through a positive feedback loop of Wnt/beta-catenin signaling. *Bone Res.* **8**, 12 (2020).
18. Suo, J. et al. The RNA-binding protein Musashi2 governs osteoblast-adipocyte lineage commitment by suppressing PPARgamma signaling. *Bone Res.* **10**, 31 (2022).
19. Yu, L., Xie, M., Zhang, F., Wan, C. & Yao, X. TM9SF4 is a novel regulator in lineage commitment of bone marrow mesenchymal stem cells to either osteoblasts or adipocytes. *Stem Cell Res. Ther.* **12**, 573 (2021).
20. Yang, X. et al. Conditional ablation of MAPK7 expression in chondrocytes impairs endochondral bone formation in limbs and adaptation of chondrocytes to hypoxia. *Cell Biosci.* **10**, 103 (2020).
21. Gong, Y. et al. Vangl2 limits chaperone-mediated autophagy to balance osteogenic differentiation in mesenchymal stem cells. *Dev. Cell* **56**, 2103–2120 (2021).
22. Cao, H. et al. PDGF-BB prevents destructive repair and promotes reparative osteogenesis of steroid-associated osteonecrosis of the femoral head in rabbits. *Bone* **167**, 116645 (2023).
23. Yin, T. The stem cell niches in bone. *J. Clin. Investig.* **116**, 1195–1201 (2006).
24. Li, C. et al. M13, an anthraquinone compound isolated from *Morinda officinalis* promotes the osteogenic differentiation of MSCs by targeting Wnt/ β -catenin signaling. *Phytomedicine* **108**, 154542 (2023).
25. Parfitt, A. M. et al. Bone histomorphometry: standardization of nomenclature, symbols, and units. *J. Bone Mineral Res.* **2**, 595–610 (1987).
26. Li, J. et al. Genetic detection of two novel LRP5 pathogenic variants in patients with familial exudative vitreoretinopathy. *BMC Ophthalmol.* **23**, 489 (2023).
27. Cai, Z. et al. Directed differentiation of human induced pluripotent stem cells to heart valve cells. *Circulation* **149**, 1435–1456 (2024).
28. Iezaki, T. et al. The MAPK Erk5 is necessary for proper skeletogenesis involving a Smurf-Smad-Sox9 molecular axis. *Development* **145**, dev164004 (2018).
29. Hoover, M. Y. et al. Purification and functional characterization of novel human skeletal stem cell lineages. *Nat. Protoc.* **18**, 2256–2282 (2023).
30. Nusse, R. & Clevers, H. Wnt/beta-catenin signaling, disease, and emerging therapeutic modalities. *Cell* **169**, 985–999 (2017).
31. Almalki, S. G. & Agrawal, D. K. Key transcription factors in the differentiation of mesenchymal stem cells. *Differentiation* **92**, 41–51 (2016).
32. Gajos-Michniewicz, A. & Czyz, M. WNT signaling in melanoma. *Int. J. Mol. Sci.* **21**, 4852 (2020).
33. Clevers, H. & Nusse, R. Wnt/beta-catenin signaling and disease. *Cell* **149**, 1192–1205 (2012).
34. Laudes, M. Role of WNT signalling in the determination of human mesenchymal stem cells into preadipocytes. *J. Mol. Endocrinol.* **46**, R65–R72 (2011).
35. Fan, Y. et al. Parathyroid hormone directs bone marrow mesenchymal cell fate. *Cell Metab.* **25**, 661–672 (2017).
36. Cong, Q. et al. p38 α MAPK regulates lineage commitment and OPG synthesis of bone marrow stromal cells to prevent bone loss under physiological and pathological conditions. *Stem Cell Rep.* **6**, 566–578 (2016).
37. Adam, C. et al. The MEK5/ERK5 mitogen-activated protein kinase cascade is an effector pathway of bone-sustaining bisphosphonates that regulates osteogenic differentiation and mineralization. *Bone* **111**, 49–58 (2018).
38. Li, Q., Xu, R., Lei, K. & Yuan, Q. Insights into skeletal stem cells. *Bone Res.* **10**, 61 (2022).
39. Liu, H. et al. Prrx1 marks stem cells for bone, white adipose tissue and dermis in adult mice. *Nat. Genet.* **54**, 1946–1958 (2022).
40. Logan, M. et al. Expression of Cre Recombinase in the developing mouse limb bud driven by a Prxl enhancer. *Genesis* **33**, 77–80 (2002).
41. Horie, T. et al. Erk5 in bone marrow mesenchymal stem cells regulates bone homeostasis by preventing osteogenesis in adulthood. *Stem Cells* **40**, 411–422 (2022).
42. Yang, R. et al. 1,25-Dihydroxyvitamin D protects against age-related osteoporosis by a novel VDR-Ezh2-p16 signal axis. *Aging Cell* **19**, e13095 (2020).
43. Wu, C. et al. Mapk7 deletion in chondrocytes causes vertebral defects by reducing MEF2C/PTEN/AKT signaling. *Genes Dis.* **11**, 964–977 (2023).
44. KS, L. et al. Extracellular vesicles from adipose tissue-derived stem cells alleviate osteoporosis through osteoprotegerin and miR-21-5p. *J. Extracell. Vesicles* **10**, e12152 (2021).
45. Horie, T. et al. Erk5 in bone marrow mesenchymal stem cells regulates bone homeostasis by preventing osteogenesis in adulthood. *Stem Cells (Dayton, OH)* **40**, 411–422 (2022).
46. Jiang, W. et al. Extracellular signal regulated kinase 5 promotes cell migration, invasion and lung metastasis in a FAK-dependent manner. *Protein Cell* **11**, 825–845 (2020).
47. Nishimoto, S. & Nishida, E. MAPK signalling: ERK5 versus ERK1/2. *EMBO Rep.* **7**, 782–786 (2006).
48. Lee, D. S. et al. NFI-C regulates osteoblast differentiation via control of osterix expression. *Stem Cells* **32**, 2467–2479 (2014).
49. Copp, G., Robb, K. P. & Viswanathan, S. Culture-expanded mesenchymal stromal cell therapy: does it work in knee osteoarthritis? A pathway to clinical success. *Cell. Mol. Immunol.* **20**, 626–650 (2023).

Acknowledgements

This work was supported by the National Natural Science Foundation of China (Nos. 82472388, 82172376, and 82330074). Guangzhou Science and Technology Project (No. 2023B03J0137). Guangdong Province Basic and Applied Basic Research Fund Project (No. 2023A1515010307).

Author contributions

Chuan Li, Jiahui Long, and Shuqing Chen: Methodology, data curation, writing-original draft. Liru Tian and Ya Xiao: Methodology and software. Shulin Chen and Deying Su: Investigation. Baolin Zhang: Statistical analyses. Peiqiang Su, Zhiheng Liao, and Caixia Xu: Conceptualization, supervision, writing-review & editing, funding acquisition.

Competing interests

The authors declare no competing interests.

Ethics approval

The animal experiments for this study were conducted at the Laboratory Animal Center of Sun Yat-sen University, approved and regulated by the Committee for the Management and Use of Laboratory Animals of Sun Yat-sen University (Approval No. SYSU-IACUC-2022-001823), and all experimental procedures were carried out in compliance with relevant regulations.

Additional information

Supplementary information The online version contains supplementary material available at <https://doi.org/10.1038/s42003-025-07765-x>.

Correspondence and requests for materials should be addressed to Peiqiang Su, Liao Zhiheng or Caixia Xu.

Peer review information *Communications Biology* thanks Gretl Hendrickx and the other, anonymous, reviewer(s) for their contribution to the peer review of this work. Primary Handling Editors: Martina Rauner and Joao Valente. A peer review file is available.

Reprints and permissions information is available at <http://www.nature.com/reprints>

Publisher's note Springer Nature remains neutral with regard to jurisdictional claims in published maps and institutional affiliations.

Open Access This article is licensed under a Creative Commons Attribution-NonCommercial-NoDerivatives 4.0 International License, which permits any non-commercial use, sharing, distribution and reproduction in any medium or format, as long as you give appropriate credit to the original author(s) and the source, provide a link to the Creative Commons licence, and indicate if you modified the licensed material. You do not have permission under this licence to share adapted material derived from this article or parts of it. The images or other third party material in this article are included in the article's Creative Commons licence, unless indicated otherwise in a credit line to the material. If material is not included in the article's Creative Commons licence and your intended use is not permitted by statutory regulation or exceeds the permitted use, you will need to obtain permission directly from the copyright holder. To view a copy of this licence, visit <http://creativecommons.org/licenses/by-nc-nd/4.0/>.

© The Author(s) 2025